ACS APPLIED MATERIALS & INTERFACES

www.acsami.org

Research Article

Flexible and Robust Biomaterial Microstructured Colored Textiles for Personal Thermoregulation

Jiawei Wu, Run Hu, Shaoning Zeng, Wang Xi, Shiyao Huang, Junhui Deng, and Guangming Tao*

Cite This: *ACS Appl. Mater. Interfaces* 2020, 12, 19015−19022

Read Online

ACCESS | Metrics & More | Article Recommendations | Supporting Information

ABSTRACT: Integrating personal thermoregulation technologies into wearable textiles has enabled extensive and profound technological breakthroughs in energy savings, thermal comfort, wearable electronics, intelligent fabrics, and so forth. Nevertheless, previous studies have suffered from long-standing issues such as limited working temperature, poor comfort, and weak reliability of the textiles. Here, we demonstrate a skin-friendly personal insulation textile and a thermoregulation textile that can perform both passive heating and cooling using the same piece of textile with zero energy input. The insulation textile material is composed of biomaterial microstructured fibers that exhibit good thermal insulation, low thermal emissivity, and good dyeability. By filling these microstructure fibers with biocompatible phase-change materials and coating them with polydimethylsiloxane, the insulation textile becomes a thermoregulation textile that shows good water hydrophobicity, high mechanical robustness, and high working stability. The proposed thermoregulation textile exhibits slow heating/cooling rates with improved thermal comfort, offering feasible and adaptive options for personal cooling/heating scenarios and enabling scalable manufacturing for practical applications.

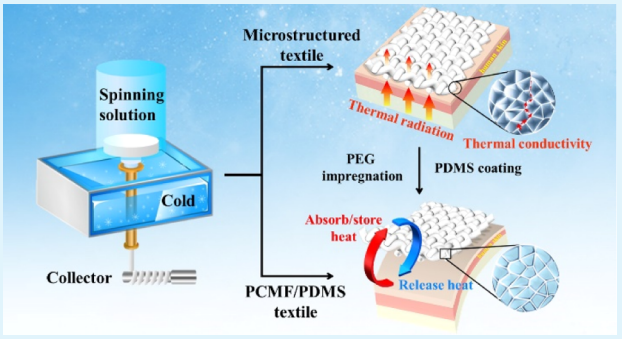

KEYWORDS: *personal thermoregulation, microstructure fiber, phase-change materials, robustness fiber, colored fiber*

INTRODUCTION

Personal thermal management (PTM) technologies that aim at only locally heating or cooling the human body without wasting excess energy for space heating or cooling through building heating, ventilation, and air conditioning (HVAC) systems have gained widespread attention and interest owing to their great potential to maintain individual comfort in a high-efficiency and energy-saving way.[1,2] For instance, with a PTM device, an increase of 2.8 °C (from 22.2 to 25 °C) of the cooling set point of an HVAC system can conserve over 25% of the energy needed for cooling while maintaining the same body temperature.[3] Conversely, reducing the heating set point from 21.1 to 20 °C can conserve as much as 34% of terminal heating energy.[3] Moreover, traditional space cooling/heating methods fail to consider the diverse requirements among individuals, which is another merit of PTM in that it can regulate individual heat preferences. Besides regulating personal thermal comfort, PTM can also be used for thermal functionalities such as thermal camouflage. Integrating PTM into wearable textiles can improve personal thermal comfort while saving energy in our daily lives and being used in military.[4−7]

Traditional PTM technologies, including active air-/liquid-cooling textiles and wearable heating textiles, can work for personal cooling or heating separately but suffer from their intrinsic drawbacks, such as bulky size, heavy weight, limited working duration, power consumption, high cost, and weak reliability. A major breakthrough was reported in 2015 by strengthening the ability for radiative cooling with textiles for personal cooling[8,9] or by suppressing radiative cooling for personal heating. Another strategy is to tune the heat conduction by either suppressing thermal conduction with aerogels[10] and porous structure textiles for personal heating and insulation[11] or enhancing thermal conduction with thermally conductive textiles for personal cooling.[12] These strategies can achieve passive personal cooling or heating separately but may fail to adapt to changes in the environment. For instance, radiative cooling technologies need a cold source (outer space or a preset low room temperature) to radiate body heat; otherwise, these technologies not only fail to dissipate body heat but also absorb a lot of heat from the environment according to Kirchhoff's law. Therefore, it is of great importance to integrate the functions of cooling and

Received: February 6, 2020
Accepted: March 27, 2020
Published: March 27, 2020

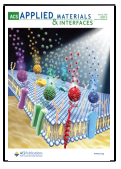

https://dx.doi.org/10.1021/acsami.0c02300
ACS Appl. Mater. Interfaces 2020, 12, 19015−19022

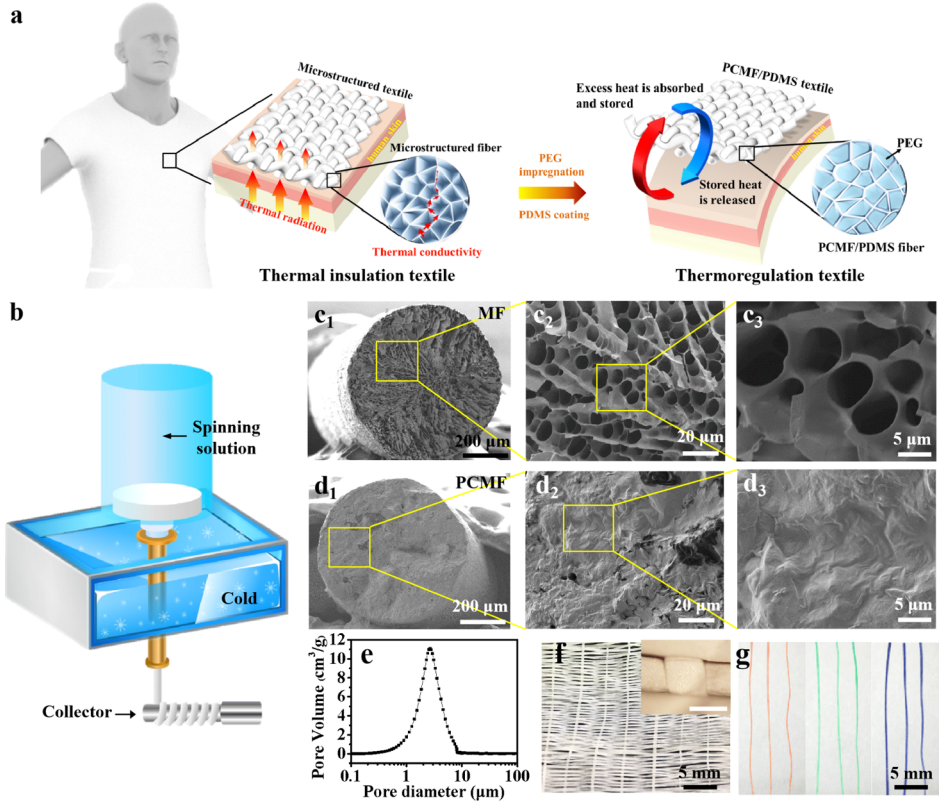

Figure 1. Illustration of the working principle and microstructure characterizations. (a) Schematic illustration of the fabrication process of the thermal insulation and thermoregulation textiles. (b) Schematic of the MF preparation. SEM images of the cross section of the MF (c_1–c_3) before and (d_1–d_3) after PEG impregnation. (e) Pore size distribution curve of MFs. (f) Photographs and optical microscopy image of a textile woven from the MF (inset, scale bar = 500 μm). (g) Photographs of the colored MFs (from left to right: red, green, and blue).

heating into one piece of textile to adapt to a capricious climate. Cui et al. developed a dual-mode textile for personal cooling and heating, but it needs to be flipped over repeatedly to adapt to the environment.[13] Zhang et al. fabricated a dynamical infrared (IR)-gating textile between the cooling and heating state by temperature and humidity.[14] Chen et al.'s design involved thickness adjustable clothes according to humidity by inserting the bent polymer sheets between two fabrics.[15] However, they only work in extremely different scenarios, such as between hot/wet and cold/dry environments. Chen et al. developed a flexible and wearable thermoelectric device with active cooling/heating, which maintained skin at the comfort temperature of 32 °C, while the ambient temperature varied from 22 to 36 °C, but it requires a continuous supply of energy to maintain its normal function.[16] Another alternative is to resort to phase-change materials (PCMs), which can absorb and release thermal energy in the form of latent heat during the phase-change process.[17,18] Unfortunately, the direct combination of PCMs and fibers faces a leakage issue resulting from the easy removal of the PCMs in the blended fibers by washing, wiping, or abrasion.[19] To solve the leakage issue, microencapsulation and coaxial electrospinning have been used to fabricate phase-change fibers, but most of these fibers have poor mechanical robustness and limited PCM loads.[20−25]

In this work, we report biomaterial microstructured colored textiles that are flexible and robust to achieve reliable personal thermoregulation. The fiber is fabricated through a simple microstructural freeze-spinning process from skin-friendly, breathable, and antibacterial silk fibroin (SF). The obtained microstructure fibers (MFs) exhibit extraordinarily good thermal insulation and low IR emissivity compared with commercial thermal textiles. By filling with biocompatible poly(ethylene glycol) (PEG), the phase-change MFs (PCMFs) show superior thermal regulation properties to commercial thermal textiles. Then, the PCMFs were coated with polydimethylsiloxane (PDMS) to overcome the leakage issue of PCMs and further enhance the hydrophobic and mechanical properties. PCMF/PDMS on gloves exhibited outstanding thermal regulation abilities in cold and hot environments, validating the excellent thermal reliability and stability. The proposed thermoregulation textiles are skin-friendly and demonstrate great potential for practical PTM, offering feasible and adaptive options for personal cooling/heating and enabling scalable manufacturing for practical applications.

RESULTS AND DISCUSSION

Fabrication and Structure Characterization. Detailed illustrations of the thermal insulation textile and thermal regulation textile are shown in Figure 1a. The basic element for the textiles is the MF. To fabricate the MF, as shown in Figure 1b, the spinning solution passes through a cold source (filled with liquid helium), the water in the solution is nucleated into ice crystals and ice particles, and the SF/chitosan (CS) solution around them is incorporated into the microstructure network in the lyophilization process, giving rise to the MFs.[26] The cross-sectional scanning electron microscopy (SEM) images of the MFs are shown in Figure 1c_1–c_3, revealing the interconnected three-dimensional microstructure networks of MFs.[27,28] To achieve PCMFs, we fill the MFs with PEG.

https://dx.doi.org/10.1021/acsami.0c02300
ACS Appl. Mater. Interfaces 2020, 12, 19015−19022

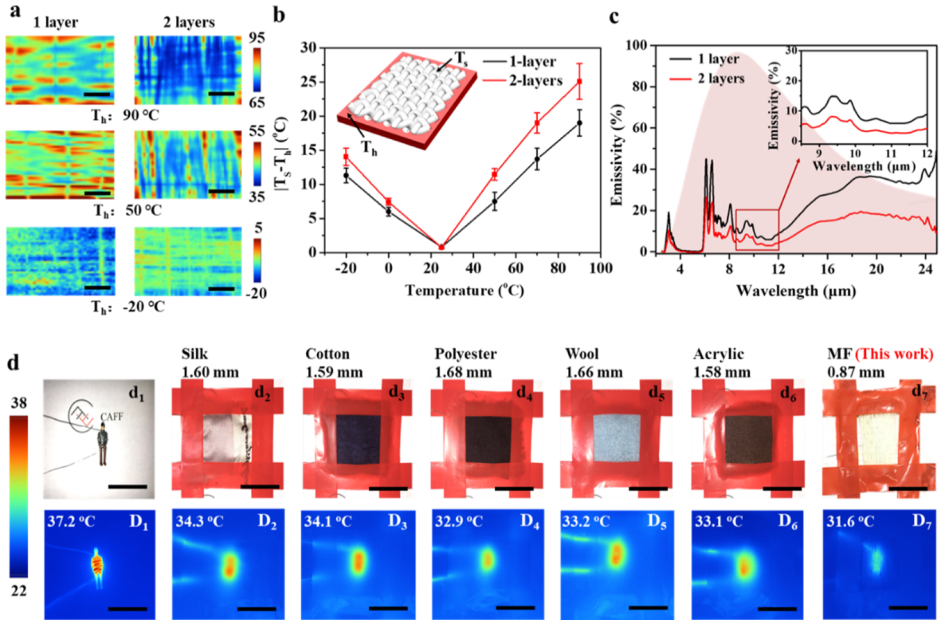

Figure 2. Characterization of thermal insulation textiles. (a) IR images of one-layer and two-layer textiles at different stage temperatures (scale bar = 5 mm). (b) Temperature difference $|T_s - T_h|$ between the textile surface and the stage vs the stage temperature for one-layer and two-layer textiles. (c) IR emissivity measurement of microstructured textiles, and the shadow denotes body radiation. (d) Photos and IR images of a humanoid model before and after covering with commercial textiles and the one-layer textile (scale bar = 20 mm).

Figure 1d_1–d_3 shows the SEM images of a PCMF, from which it is clearly observed that the microstructures in the MFs were filled in and covered by PEG. As shown in Figure 1e, the pore size distribution measured by mercury intrusion porosimetry shows that most of the pores fall into the size range of 0.6–9.1 μm, and the porosity reaches 83%. The MFs were densely woven into the textile without mechanical damage, as shown in Figure 1f. All MFs have a similar fiber diameter (500 ± 50 μm). Furthermore, the MFs can be dyed into colored MFs by adding a water-soluble dye (red, green, or blue) solution into the original blended spinning solution in a similar freeze-spinning process (Figure 1g).

Characterization of Thermal Insulation Textiles. After weaving the MFs into the textile, we placed it on a temperature-controlling stage from −20 to 90 °C. The temperature variation was recorded and measured by thermocouples attached on both the textile surface and the stage. A series of IR images were taken when the surface temperature was stable. During the measurement, the ambient temperature was kept at approximately 25 °C. Figure 2a shows that the measured temperature of the textile is much lower than that of the stage and the temperature of the two-layer textile is lower than that of the one-layer textile, when the stage temperatures are 50 and 90 °C. However, when the stage temperature is −20 °C, the two-layer textile seems warmer because of the lower conductivity. This is explained by the low intrinsic thermal conductivity of MFs and textiles. The thermocouple-measured temperature difference ($|T_s - T_h|$) between the textile surface (T_s) and the stage (T_h) in Figure 2b increases from 11 and 18 °C at the stage temperature to −20 and 90 °C, showing the superior thermal insulation at low and high temperatures. Accordingly, the two-layer textile shows better thermal insulation properties than the one-layer textile. For the two-layer textile, the temperature difference $|T_s - T_h|$ reaches 14 and 25 °C at the same stage temperature variation. As mentioned above, the porosity of the fabricated MFs is up to 83%, and heat can be conducted only through the interconnected three-dimensional network structure in the MF, leading to a low thermal conductivity of 0.033 W/(m·K). Because of the lack of obvious air convection, the two-layer textile is thicker with better thermal insulation performance.

In addition to thermal conduction, over 50% of body heat is dissipated through thermal radiation;[29] therefore, it is critical to investigate the radiative properties of MF-based textiles. The dominant thermal radiation wavelength of the human body ranges from 7 to 14 μm,[29] which is also the IR atmospheric window. The spectral emissivity curves of the one-layer and two-layer textiles are shown in Figure 2c. The shadow area indicates the emission of human body radiation according to Planck's law. Because of the comparable pore size of MFs to the IR wavelength, very intense IR scattering/reflection events occurred at the numerous solid–air interfaces, leading to high reflectivity and low absorptivity of MFs.[30] The emissivity of the one-layer textile is approximately 0.059–0.231 at the IR atmospheric window and is only 0.149 at the dominant wavelength of 9.5 μm of body radiation, which decreases to 0.075 for the two-layer textile. Compared with that of the one-layer textile, the lower-emissivity two-layer textile results in enhanced capability to shield IR radiation, which corresponds to the lower measured temperature in Figure 2a. It is the combination of lower thermal conductivity and emissivity that make the as-prepared textiles superior for thermal insulation characteristics.

To further verify the superior thermal insulation performance, we compare the steady IR images of the proposed thermal insulation textile and some commercial textiles. As shown in Figure 2d_1, a three-dimensional printed humanoid model was wrapped with a metal wire to simulate a self-heating human body. A constant current of 0.18 A and a voltage of 1.50 V were input to heat the humanoid model for 2 h to achieve the steady state at room temperature. The maximum temperature of the model was measured at 37.2 ± 0.3 °C in

https://dx.doi.org/10.1021/acsami.0c02300
ACS Appl. Mater. Interfaces 2020, 12, 19015–19022

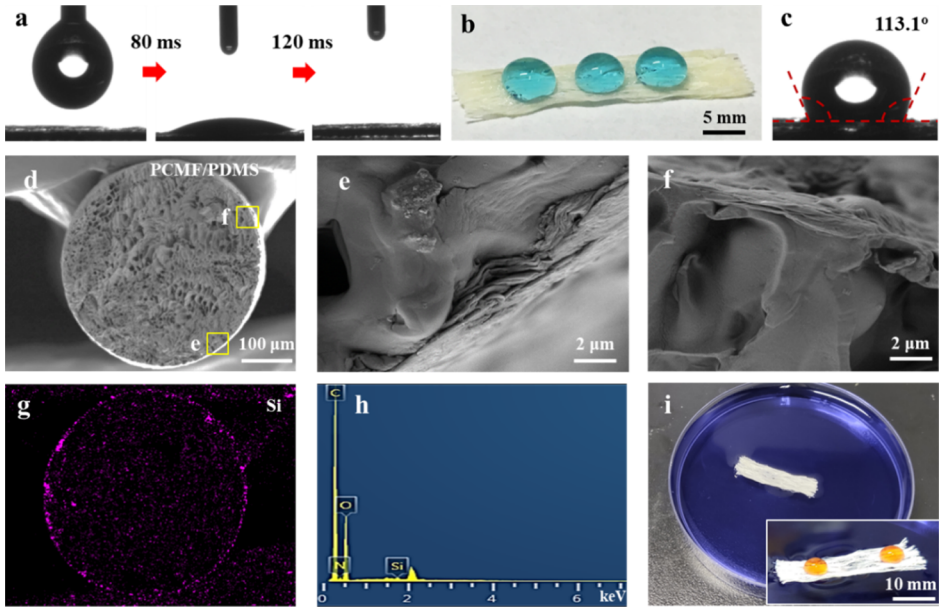

Figure 3. Hydrophobic property measurement of the PCMF/PDMS textile. (a) Water hydrophilicity measurement of the PCMF textile. (b) Photos of water droplets on the PCMF/PDMS textile. (c) Photograph of water contact angle measurements of the PCMF/PDMS textile. (d–f) SEM images of the cross section of the PCMF/PDMS fiber. (g–h) EDS element maps showing the distribution of Si in the PCMF/PDMS. (i) Photos of the PCMF/PDMS textile with water droplets on its surface and with the textile floating on water.

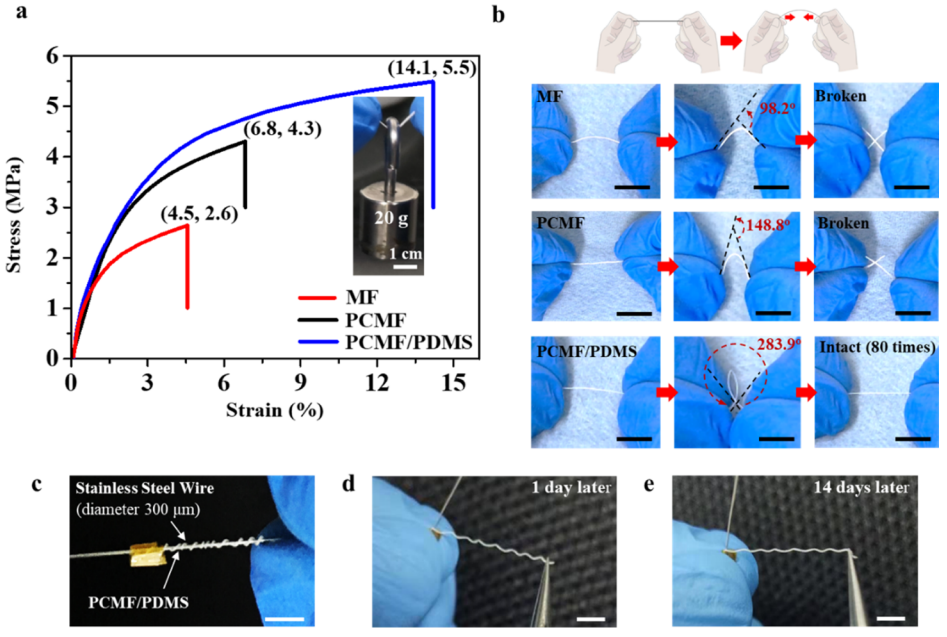

Figure 4. Mechanical characterization of the MF, PCMF, and PCMF/PDMS. (a) Tensile stress–strain curves of the MF, PCMF, and PCMF/PDMS. Photograph of a single aerogel fiber with a tensile load of 20 g (inset). (b) Schematic diagram and photographs of the MF, PCMF, and PCMF/PDMS bending performance tests (scale bar = 1 cm). (c) Photographs of PCMF/PDMS wrapped on a stainless steel wire. PCMF/PDMS released from the stainless steel wire after being wrapped for (d) 1 day and (e) 14 days (scale bar = 3 mm).

Figure 2D_1, which can be used to simulate the human body. Figure 2d_2–d_7 shows photographs of the humanoid model covered with textiles made of silk (d_2, thickness: 1.60 mm), cotton (d_3, thickness: 1.59 mm), polyester (d_4, thickness: 1.68 mm), wool (d_5, thickness: 1.66 mm), acrylic (d_6, thickness: 1.58 mm), and one-layer textile (d_7, thickness: 0.87 mm). Accordingly, Figure 2D_2–D_7 shows the IR images. Note that the thickness of the proposed textile is the smallest among the studied textiles, but its temperature is the lowest compared with these commercial thick textiles. The highest temperature of 34.3 °C is from the 1.60 mm thick silk cover (Figure 2D_2). In contrast, the highest temperature achieved with the one-layer textile is only 31.6 °C (Figure 2D_7), which is almost 2.7 °C lower than that of the silk cover. From these comparisons, it is seen that the proposed thermal insulation textile has low conductivity and emissivity for better thermal insulation performance than most commercial textiles. Furthermore, most thermal insulation materials (e.g., mineral wool, expanded polystyrene, and polyurethane) are neither skin-friendly nor biodegradable.[31] Therefore, these thermal

https://dx.doi.org/10.1021/acsami.0c02300
ACS Appl. Mater. Interfaces 2020, 12, 19015–19022

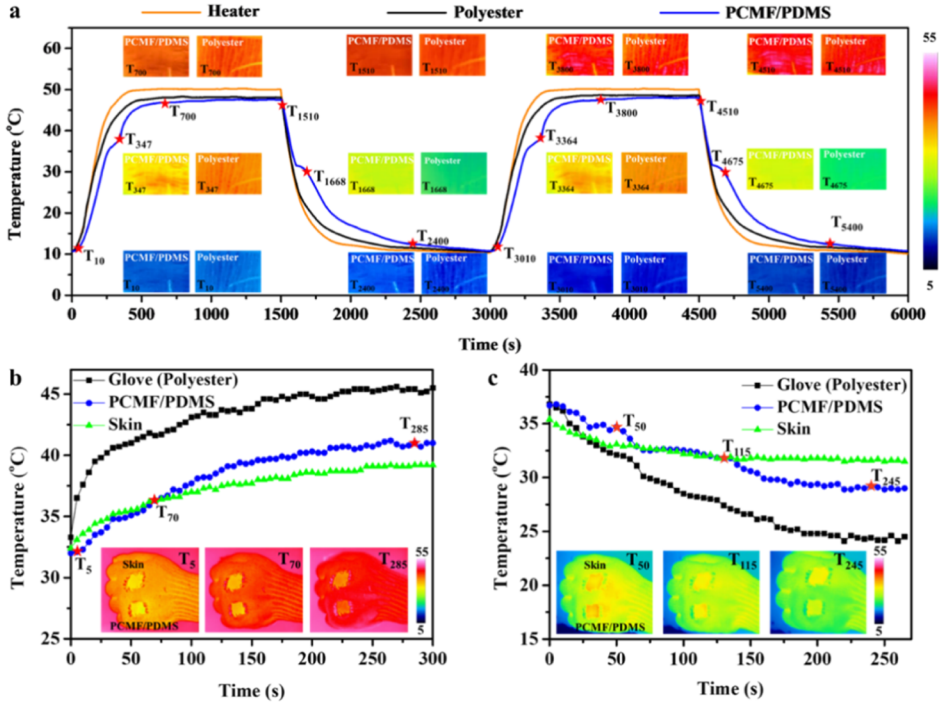

Figure 5. Thermal characterization of the thermoregulation textile. (a) Heating and cooling temperature curves of the heater, polyester, and PCMF/PDMS textiles. Insets: IR images of the textiles at different moments. (b,c) Heating and cooling temperature curves of the polyester glove, PCMF/PDMS textile, and bare skin in the calorstat at 50 and 10 °C, respectively. Insets: IR images of a human hand with the glove at different moments.

insulation textiles made of nontoxic, biodegradable, and biocompatible SF demonstrate great potential for practical PTM.

Characterization of PCMF and PCMF/PDMS. To overcome the PCM leakage issue, we coated the PCMF with PDMS to fabricate PCMF/PDMS and then wove it into the thermoregulation textile. Because of its hydrophobicity, the fabricated thermoregulation textile shows good water-repellent performance. As shown in Figure 3a, the MF-based thermal insulation textile is hydrophilic because of the hydrophilic PEG and microstructures. After coating with PDMS, the PCMF/PDMS textile becomes hydrophobic, and the contact angle is approximately 113.1° (Figure 3b,c). These hydrophobic properties make PCMF/PDMS textiles waterproof to enable more applications. Figure 3d–f shows the SEM images of the cross sections of PCMF/PDMS fibers. It can be seen that PDMS is mainly distributed on the surface of the PCMF, confirming the good coating property. To further confirm the coating uniformity, the energy-dispersive X-ray spectroscopic (EDS) elemental mapping of the cross section of PCMF/PDMS was characterized (Figure 3g,h). The distribution of the Si element in the EDS map shows a uniform distribution of PDMS on the surface of the PCMF, verifying the uniform coating to form a stable hydrophobic layer. Furthermore, the PCMF/PDMS textile with water droplets on its surface can float on water, indicating the lightweight and excellent waterproof property of this textile.

Mechanical Characterization. Figure 4 summarizes the mechanical characterization of MFs, PCMFs, and PCMF/PDMS fibers at room temperature. As shown in Figure 4a, the fracture strength and the strain of PCMFs are 4.3 MPa and 6.8%, which are 63.2 and 52.2% higher than that of MFs, respectively. It is observed that filling with PEG can contribute to an increase in the strength and toughness of MFs. After coating PDMS on the surface of PCMFs, the strength and strain of PCMFs increase from 4.3 to 5.5 MPa and from 6.8 to 14.1%, respectively. Thus, the PDMS coating further enhances both the strength and toughness of PCMFs. In addition, this fiber exhibits high mechanical strength, where a single PCMF/PDMS fiber can withstand a tensile load of 20 g (inset in Figure 4a). These results indicate that the PDMS elastomer with good mechanical properties coated on the outer surface and internal microstructure of PCMFs will significantly reduce the damage of the PCMF structure by external force and improve their mechanical properties when PCMF/PDMS is subjected to tensile force. In addition, the tensile properties of composite fibers are significantly affected by the content of their PCMs. Generally, the tensile strength of composite fibers is inversely proportional to the content of their PCMs.[32] However, PCMF/PDMS can still achieve 5.5 MPa of tensile strength with the PCM content of 86.3 wt %, which is more significant than other PCM composite fibers reported in recent years, especially those phase-change composite fibers that use biomaterials as fiber support materials (Figure S2 and Table S2 in the Supporting Information). Figure 4b–e shows photographs of the flexibility tests of MFs, PCMFs, and PCMF/PDMS fibers. As shown in Figure 4b, the MF, PCMF, and PCMF/PDMS were manually bent. The MF was broken under 98.2° bending, which was attributed to the fragile microstructure of the MF. However, when PEG was filled in the microstructure, the maximum bending angle of the PCMF was improved to 148.8° because the soft PEG in the MF could effectively help to prevent fragile microstructures from breaking. Interestingly, PCMF/PDMS showed much better flexibility than the MF and PCMF. The soft and elastic PDMS uniformly covered and filled the PCMF, which could

https://dx.doi.org/10.1021/acsami.0c02300
ACS Appl. Mater. Interfaces 2020, 12, 19015–19022

significantly increase the bending angle up to 283.9°, and PCMF/PDMS remained intact even after bending 80 times (Figure 4b). The PDMS coating not only improves the mechanical strength but also endows PCMF with excellent robustness. To further test the flexibility of PCMF/PDMS, a single PCMF/PDMS fiber was wrapped on a stainless steel wire (diameter: 300 μm) (Figure 4c). Notably, the PCMF/PDMS fiber remained intact after wrapping on the stainless steel wire for 1 and 14 days, which validates the high flexibility of PCMF/PDMS.

Characterization of Thermoregulation Textiles. Thermal insulation textiles can work to maintain thermal comfort only in harsh environments, such as extremely cold or hot environments, because of their bidirectional insulation properties. However, these thermal insulation textiles cannot maintain human thermal comfort at normal temperature range but can be used in our daily life at normal temperature range. To fill this temperature gap and promote daily wearability, we turn the biomaterial MF-based thermal insulation textile into a PCMF/PDMS-based thermoregulation textile. The well-biocompatible PEG and skin-friendly MF give this textile good wearing comfort. Meanwhile, the thermal hysteresis property of PEG during the phase-change process enables the thermoregulation function of the PCMF/PDMS-based textile to manage human body temperature because the melting temperature (39 °C) of PEG1000 is close to the temperature of the human body. The very good thermal storage, phase transition, and thermal cycle stability properties of these PCMFs and the thermal properties of PCMF/PDMS are discussed in the Supporting Information. Moreover, the temperature response is also an important parameter to measure the thermal regulation performance during heating and cooling processes. To this end, the heating and cooling temperature curves of a heater, a polyester textile, and the fabricated thermoregulation textile on the heater under a cycling heater temperature are presented in Figure 5a. When the temperature is higher than 37.7 °C during the heating process, the PCMF/PDMS textile shows a lower temperature because the solid PEG begins to melt and absorbs heat to hinder the temperature rise in the thermoregulation textile, which is consistent with the differential scanning calorimetry (DSC) curve in Figure S2 (Supporting Information). In contrast, when the temperature is lower than 31.5 °C during the cooling process, the PCMF/PDMS textile has a higher temperature in a low-temperature environment because the melted PEG begins solidification and releases heat to hinder the temperature drop in the thermoregulation textile, which corresponds to the DSC analysis result in Figure S2. Notably, the temperature curves under the two temperature cycles are maintained, validating the good thermal reliability of the thermoregulation textile. In addition, we recorded the corresponding IR images of polyester and PCMF/PDMS textiles as shown in the insets of Figure 5a, from which we can see that the temperature of PCMF/PDMS is lower during the heating process and is higher during the cooling process than that of the polyester textile. These IR image comparisons, corresponding to the thermocouple-measured temperature curves, confirm the good thermoregulation performance of the PCMF/PDMS textile.

To further illustrate the thermoregulation performance of the proposed PCMF/PDMS textile for human body, we integrated a piece of 2.5 cm × 3.1 cm × 0.89 mm textile into a polyester glove by weaving. A same-size hole was cut in the polyester glove to observe the bare skin. After wearing this glove, we put the hand in a calorstat with constant temperatures of 50 and 10 °C to observe the temperature variations, which are shown in Figure 5b,c, respectively. When the temperature is higher and lower than the phase-change temperature, an obvious thermal hysteresis phenomenon is observed, which is consistent with the result shown in Figure 5a. Compared with the 2.25 mm thick polyester glove, the 0.89 mm thick PCMF/PDMS textile demonstrates better thermoregulation performance, that is, it has a lower temperature during the heating process and a higher temperature during the cooling process. The bare skin temperature, as a reference temperature, is more stable than that of the textiles because of the metabolic modulation of the human body. However, when wearing the PCMF/PDMS thermoregulation textile, the heat absorbed and released by PEG can buffer the ambient temperature change and extend the thermal comfort time up to 70 s for the human body. Simultaneously, the corresponding IR images of the glove, skin, and PCMF/PDMS shown in the insets of Figure 5b,c also clearly demonstrate the thermal hysteresis phenomenon of the PCMF/PDMS textile for thermal regulation.

CONCLUSIONS

Biomaterial microstructured colored textiles that are flexible and robust were produced from SF through a controllable microstructural freeze-spinning technique. Because of the three-dimensional interconnected microstructure, the obtained fibers demonstrate low thermal conductivity, low IR emissivity, and good dyeability, and the fiber-woven textiles exhibit superior thermal insulation property compared with many commercial textiles. By filling these MFs with biocompatible PCMs and coating with PDMS, we turn the thermal insulation textile into thermoregulation textiles, which show good water hydrophobicity, superior mechanical robustness, and high working stability. Furthermore, the proposed thermoregulation textile exhibits slow heating and cooling rates than the polyester glove in 50 and 10 °C isothermal environments and can significantly extend the skin comfort time up to 70 and 115 s, respectively. In addition, the proposed thermoregulation textile can be further extended to achieve different temperature applications through filling different phase-changing materials. The materials and fabrication process are compatible with the existing textile industry, and the thermal, wearable, and mechanical performances are satisfying, enabling and promoting large-scale mass production for practical personal thermoregulation applications.

METHODS

Materials. Silkworm cocoons were purchased from Yiwu Ruiheng Co., Ltd, China. CS (high viscosity, >400 mPa s) was purchased from Aladdin Chemistry Co., Ltd, China. PEG (1000, 99% pure) was purchased from Usolf Chemical Technology Co., Ltd, China. PDMS was purchased from SINWE Co., Ltd, China. Water-soluble dye was obtained from Xindi Dye Co., Ltd, China.

Preparation of SF and CS Solutions. A silkworm cocoon (5 g) was boiled for 30 min in an aqueous solution of 0.02 M Na_2CO_3 (Sinopharm Chemical Reagent Co., Ltd, China) and then rinsed completely with distilled water to extract the sericin proteins. Before dissolving in LiBr solution, the extracted SF was dried in a fume hood overnight. The dried degummed silk was then directly dissolved in a 9.3 M LiBr (Sigma-Aldrich, USA) solution at 60 °C for 4 h. Subsequently, the solution was dialyzed for 2 days in distilled water at room temperature using a Slide-A-Lyzer dialysis bag (molecular

https://dx.doi.org/10.1021/acsami.0c02300
ACS Appl. Mater. Interfaces 2020, 12, 19015−19022

weight cutoff = 3500, Pierce, USA). After removing LiBr, the solution in the dialysis bag was centrifuged using a Xiangyi TGL-16M centrifuge (Changsha, China) at 11,000 rpm at 4 °C for 3 × 20 min to remove any white flocculent or brown matter. The concentration of SF was determined by measuring the ratio of the volume of SF solution to the weight of dried SF.

The CS solution was prepared by dissolving 1 g of CS powder in 20 mL of a 1% glacial acetic acid (Sinopharm Chemical Reagent Co., Ltd, China) aqueous solution at 60 °C.

Preparation of the Spinning Solution. A spinning solution containing SF and CS (W_{SF}/W_{CS} = 9:1) was carefully mixed at room temperature. After stirring for 1 h, the solution was centrifuged at 11,000 rpm at 4 °C for 20 min to eliminate bubbles and then concentrated to a suitable concentration (100 mg/mL) using a vacuum oven at 50 °C.

MF Preparation. As shown in Figure 1b, the MF was prepared by the freeze-spinning method. A copper tube connected to a liquid nitrogen bath was used as the cold source. The spinning solution was extruded from a syringe at a constant speed. When it slowly passed through the cold copper tube, the solution was gradually frozen, and the frozen fiber was further collected using a fiber collector. The collected frozen fibers were ultimately lyophilized for 2−3 days at −70 °C under 0.01 mbar pressure with a freeze drier (LGJ-18, Beijing, China) until all of the water in the frozen fibers was completely removed.

Colored Microstructured Fiber Preparation. The MF was colored by adding a water-soluble dye [red (sample name: 773 weak acid rose-red B), green (sample name: 775 weak acid green 7G), and blue (sample name: 774 weak acid blue MB)] solution into the blended spinning solution, followed by freeze-spinning.

PCMF and PCMF/PDMS Preparation. The MFs were submerged into melted PEG in an oven at 80 °C for 6 h for PEG to infuse into the fiber pores. After that, the PC fibers were transferred onto the filter paper to remove the excess PEG adhered on the surface at 80 °C; this step was repeated several times. After cooling to room temperature and coating with PDMS, the PCMF and PCMF/PDMS were obtained.

Characterization on Morphology and Mechanical Properties. The cross sections of the fibers were observed with a Gemini 300 (ZEISS, Germany) scanning electron microscope at an acceleration voltage of 3 kV. The images of the microstructured textile were obtained using a metalloscope (CX40M, China). The mechanical properties were tested in tensile mode by a dynamic mechanical analysis machine (TA Q800, USA) with a gauge length of 10 mm at a loading rate of 0.5 mm/min. At least five samples were tested for each experimental condition to obtain statistically reliable values. Fourier transform IR (FTIR) spectrometry was performed by a Nicolet 6700 FTIR spectrometer (Thermo Electron, USA) equipped with a diffuse integrating sphere (Labsphere RTC-060-IG, USA), and its spectrum ranged from 400 to 4000 cm^{-1}. The IR emissivity of the microstructured textile was calculated on the basis of emissivity = 100% − reflectivity − transmissivity. The thermal properties, including thermal stability, phase-change temperature, and enthalpy of the PCFs, were studied using a Q2000 (TA instruments, USA) differential scanning calorimeter at a heating and cooling rate of 10 °C min^{-1} and under flowing nitrogen at 50 mL min^{-1}. X-ray diffraction (XRD) patterns were collected at ambient temperature with a scanning rate of 2°/min over an angular range of 5°−60° (2θ). Thermal gravimetric analysis (TGA) was carried out using a TG analyzer (Mettler Toledo, USA) with a heating rate of 10 °C min^{-1} in a nitrogen atmosphere.

Characterization on Thermal Insulation and Thermoregulation Properties. The IR thermal images were taken by a Fluke (Ti400, USA) camera. The working distance was approximately 30 cm. During the IR experiment, the IR emissivity of the samples is calibrated with thermocouples. The temperatures of the samples were monitored and recorded by thermal couples connected to a temperature controller. The thermal conductivity of the MFs was measured with a hot disk thermal conductivity meter (TPS2500S, Sweden). Before testing, the specimen was first dried for 24 h at 60 °C in vacuum to remove moisture in the pores. The heating and cooling temperature curves of the polyester glove, PCMF/PDMS textile, and bare skin are tested in the calorstat at 50 and 10 °C, respectively.

■ ASSOCIATED CONTENT

Supporting Information

The Supporting Information is available free of charge at https://pubs.acs.org/doi/10.1021/acsami.0c02300.

SEM images, FTIR spectra, XRD patterns, and TGA and DSC curves (PDF)

■ AUTHOR INFORMATION

Corresponding Author

Guangming Tao − *Wuhan National Laboratory for Optoelectronics and School of Optical and Electronic Information, Huazhong University of Science and Technology, Wuhan 430074, China;* orcid.org/0000-0002-1371-7735; Email: tao@hust.edu.cn

Authors

Jiawei Wu − *Wuhan National Laboratory for Optoelectronics and School of Optical and Electronic Information, Huazhong University of Science and Technology, Wuhan 430074, China*

Run Hu − *State Key Laboratory of Coal Combustion, School of Energy and Power Engineering, Huazhong University of Science and Technology, Wuhan 430074, China;* orcid.org/0000-0003-0274-9982

Shaoning Zeng − *Wuhan National Laboratory for Optoelectronics and School of Optical and Electronic Information, Huazhong University of Science and Technology, Wuhan 430074, China*

Wang Xi − *State Key Laboratory of Coal Combustion, School of Energy and Power Engineering, Huazhong University of Science and Technology, Wuhan 430074, China*

Shiyao Huang − *State Key Laboratory of Coal Combustion, School of Energy and Power Engineering, Huazhong University of Science and Technology, Wuhan 430074, China*

Junhui Deng − *Wuhan National Laboratory for Optoelectronics and School of Optical and Electronic Information, Huazhong University of Science and Technology, Wuhan 430074, China*

Complete contact information is available at: https://pubs.acs.org/10.1021/acsami.0c02300

Author Contributions

J.W. and R.H. contributed equally. G.T. and R.H. conceived the study and wrote the manuscript with inputs from all authors. J.W., S.H., S.Z., J.D., and W.X. performed experiments.

Notes

The authors declare no competing financial interest.

■ ACKNOWLEDGMENTS

The authors would like to acknowledge Xinliang Zhang and Jun Zhou for their encouragement, support, and vision. G.T. acknowledges the support of the National Natural Science Foundation of China (grant no. 61875064) and the WNLO Man-Machine Lab Fund. R.H. acknowledges the support of the National Natural Science Foundation of China (grant no. 51606074).

REFERENCES

(1) Hsu, P.-C.; Song, A. Y.; Catrysse, P. B.; Liu, C.; Peng, Y.; Xie, J.; Fan, S.; Cui, Y. Radiative Human Body Cooling by Nanoporous Polyethylene Textile. *Science* **2016**, *353*, 1019−1023.

(2) Yang, A.; Cai, L.; Zhang, R.; Wang, J.; Hsu, P.-C.; Wang, H.; Zhou, G.; Xu, J.; Cui, Y. Thermal Management in Nanofiber-Based Face Mask. *Nano Lett.* **2017**, *17*, 3506−3510.

(3) Hoyt, T.; Kwang, L. H.; Zhang, H.; Arens, E.; Webster, T. Energy Savings from Extended Air Temperature Setpoints and Reductions in Room Air Mixing. *Int. Conf. Environ. Ergon.* **2009**, 608.

(4) Yazdi, M.; Sheikhzadeh, M. Personal Cooling Garments: a Review. *J. Text. Inst.* **2014**, *105*, 1231−1250.

(5) Hu, J.; Meng, H.; Li, G.; Ibekwe, S. I. A Review of Stimuli-responsive Polymers for Smart Textile Applications. *Smart Mater. Struct.* **2012**, *21*, 053001.

(6) Luo, H.; Li, Q.; Du, K.; Xu, Z.; Zhu, H.; Liu, D.; Cai, L.; Ghosh, P.; Qiu, M. An Ultra-thin Colored Textile with Simultaneous Solar and Passive Heating Abilities. *Nano Energy* **2019**, *65*, 103998.

(7) Hu, R.; Zhou, S.; Li, Y.; Lei, D.-Y.; Luo, X.; Qiu, C.-W. Illusion Thermotics. *Adv. Mater.* **2018**, *30*, 1707237.

(8) Tong, J. K.; Huang, X.; Boriskina, S. V.; Loomis, J.; Xu, Y.; Chen, G. Infrared-Transparent Visible-Opaque Fabrics for Wearable Personal Thermal Management. *ACS Photonics* **2015**, *2*, 769−778.

(9) Cai, L.; Song, A. Y.; Li, W.; Hsu, P.-C.; Lin, D.; Catrysse, P. B.; Liu, Y.; Peng, Y.; Chen, J.; Wang, H.; Xu, J.; Yang, A.; Fan, S.; Cui, Y. Spectrally Selective Nanocomposite Textile for Outdoor Personal Cooling. *Adv. Mater.* **2018**, *30*, 1802152.

(10) Zhan, H.-J.; Wu, K.-J.; Hu, Y.-L.; Liu, J.-W.; Li, H.; Guo, X.; Xu, J.; Yang, Y.; Yu, Z.-L.; Gao, H.-L.; Luo, X.-S.; Chen, J.-F.; Ni, Y.; Yu, S.-H. Biomimetic Carbon Tube Aerogel Enables Super-Elasticity and Thermal Insulation. *Chem* **2019**, *5*, 1871−1882.

(11) Cui, Y.; Gong, H.; Wang, Y.; Li, D.; Bai, H. A Thermally Insulating Textile Inspired by Polar Bear Hair. *Adv. Mater.* **2018**, *30*, 1706807.

(12) Gao, T.; Yang, Z.; Chen, C.; Li, Y.; Fu, K.; Dai, J.; Hitz, E. M.; Xie, H.; Liu, B.; Song, J.; Yang, B.; Hu, L. Three-Dimensional Printed Thermal Regulation Textiles. *ACS Nano* **2017**, *11*, 11513−11520.

(13) Hsu, P.-C.; Liu, C.; Song, A. Y.; Zhang, Z.; Peng, Y.; Xie, J.; Liu, K.; Wu, C.-L.; Catrysse, P. B.; Cai, L.; Zhai, S.; Majumdar, A.; Fan, S.; Cui, Y. A Dual-mode Textile for Human Body Radiative Heating and Cooling. *Sci. Adv.* **2017**, *3*, No. e1700895.

(14) Zhang, X. A.; Yu, S.; Xu, B.; Li, M.; Peng, Z.; Wang, Y.; Deng, S.; Wu, X.; Wu, Z.; Ouyang, M.; Wang, Y. Dynamic Gating of Infrared Radiation in a Textile. *Science* **2019**, *363*, 619.

(15) Zhong, Y.; Zhang, F.; Wang, M.; Gardner, C. J.; Kim, G.; Liu, Y.; Leng, J.; Jin, S.; Chen, R. Reversible Humidity Sensitive Clothing for Personal Thermoregulation. *Sci. Rep.* **2017**, *7*, 44208.

(16) Hong, S.; Gu, Y.; Seo, J. K.; Wang, J.; Liu, P.; Meng, Y. S.; Xu, S.; Chen, R. Wearable Thermoelectrics for Personalized Thermoregulation. *Sci. Adv.* **2019**, *5*, No. eaaw0536.

(17) Zhou, Y.; Liu, X.; Sheng, D.; Lin, C.; Ji, F.; Dong, L.; Xu, S.; Wu, H.; Yang, Y. Polyurethane-based Solid-solid Phase Change Materials with In Situ Reduced Graphene Oxide for Light-thermal Energy Conversion and Storage. *Chem. Eng. J.* **2018**, *338*, 117−125.

(18) Zhang, X.; Liu, H.; Huang, Z.; Yin, Z.; Wen, R.; Min, X.; Huang, Y.; Liu, Y.; Fang, M.; Wu, X. Preparation and Characterization of the Properties of Polyethylene Glycol @ Si_3N_4 Nanowires as Phase-change Materials. *Chem. Eng. J.* **2016**, *301*, 229−237.

(19) Cherif, C.; Tran, N. H. A.; Kirsten, M.; Bruenig, H.; Vogel, R. Environmentally Friendly and Highly Productive Bi-component Melt Spinning of Thermoregulated Smart Polymer Fibres with High Latent Heat Capacity. *Express Polym. Lett.* **2018**, *12*, 203−214.

(20) Liu, C.; Rao, Z.; Zhao, J.; Huo, Y.; Li, Y. Review on Nanoencapsulated Phase Change Materials: Preparation, Characterization and Heat Transfer Enhancement. *Nano Energy* **2015**, *13*, 814−826.

(21) Do, T.; Ko, Y. G.; Chun, Y.; Choi, U. S. Encapsulation of Phase Change Material with Water-Absorbable Shell for Thermal Energy Storage. *ACS Sustain. Chem. Eng.* **2015**, *3*, 2874−2881.

(22) Lu, Y.; Xiao, X.; Fu, J.; Huan, C.; Qi, S.; Zhan, Y.; Zhu, Y.; Xu, G. Novel Smart Textile with Phase Change Materials Encapsulated Core-sheath Structure Fabricated by Coaxial Electrospinning. *Chem. Eng. J.* **2019**, *355*, 532−539.

(23) Babapoor, A.; Karimi, G.; Golestaneh, S. I.; Mezjin, M. A. Coaxial Electro-spun PEG/PA6 Composite Fibers: Fabrication and Characterization. *Appl. Therm. Eng.* **2017**, *118*, 398−407.

(24) Zdraveva, E.; Fang, J.; Mijovic, B.; Lin, T. Electrospun Poly(vinyl alcohol)/Phase Change Material Fibers: Morphology, Heat Properties, and Stability. *Ind. Eng. Chem. Res.* **2015**, *54*, 8706−8712.

(25) Li, X.; Sanjayan, J. G.; Wilson, J. L. Fabrication and Stability of Form-stable Diatomite/paraffin Phase Change Material Composites. *Energ. Buildings* **2014**, *76*, 284−294.

(26) Li, M.; Minoura, N.; Dai, L.; Zhang, L. Preparation of Porous Poly(vinyl alcohol)-Silk Fibroin (PVA/SF) Blend Membranes. *Macromol. Mater. Eng.* **2001**, *286*, 529−533.

(27) Bai, H.; Chen, Y.; Delattre, B.; Tomsia, A. P.; Ritchie, R. O. Bioinspired Large-scale Aligned Porous Materials Assembled with Dual Temperature Gradients. *Sci. Adv.* **2015**, *1*, No. e1500849.

(28) Bai, H.; Walsh, F.; Gludovatz, B.; Delattre, B.; Huang, C.; Chen, Y.; Tomsia, A. P.; Ritchie, R. O. Bioinspired Hydroxyapatite/Poly(methyl methacrylate) Composite with a Nacre-Mimetic Architecture by a Bidirectional Freezing Method. *Adv. Mater.* **2016**, *28*, 50−56.

(29) Hardy, J. D.; Dubois, E. F. Regulation of Heat Loss from the Human Body. *Proc. Natl. Acad. Sci. U.S.A.* **1937**, *23*, 624−631.

(30) Ahn, J.; Lim, T.; Yeo, C. S.; Hong, T.; Jeong, S.-M.; Park, S. Y.; Ju, S. Infrared Invisibility Cloak Based on Polyurethane-Tin Oxide Composite Microtubes. *ACS Appl. Mater. Interfaces* **2019**, *11*, 14296−14304.

(31) Jelle, B. P. Traditional, State-of-the-art and Future Thermal Building Insulation Materials and Solutions - Properties, Requirements and Possibilities. *Energ. Buildings* **2011**, *43*, 2549−2563.

(32) Chen, C.; Wang, L.; Huang, Y. Electrospun Phase Change Fibers based on Polyethylene Glycol/cellulose Acetate Blends. *Appl. Energy* **2011**, *88*, 3133−3139.

https://dx.doi.org/10.1021/acsami.0c02300
ACS Appl. Mater. Interfaces 2020, 12, 19015−19022